Title
Spatial correlation of shear-wave velocity in the San Francisco Bay Area sediments

Journal
Soil Dynamics and Earthquake Engineering, 27(2)

ISSN
02677261

Authors
Thompson, Eric M
Baise, Laurie G
Kayen, Robert E

Publication Date
2007-02-01

DOI
10.1016/j.soildyn.2006.05.004

Peer reviewed

ELSEVIER

Soil Dynamics and Earthquake Engineering 27 (2007) 144–152

SOIL DYNAMICS AND EARTHQUAKE ENGINEERING

www.elsevier.com/locate/soildyn

Spatial correlation of shear-wave velocity in the San Francisco Bay Area sediments

Eric M. Thompson[a,*], Laurie G. Baise[a], Robert E. Kayen[b]

[a]*Department of Civil and Environmental Engineering, Tufts University, 200 College Avenue, Medford, MA 02155, USA*
[b]*US Geological Survey, 345 Middlefield Rd., MS-999, Menlo Park, CA 94025, USA*

Received 7 April 2006; received in revised form 29 April 2006; accepted 2 May 2006

Abstract

Ground motions recorded within sedimentary basins are variable over short distances. One important cause of the variability is that local soil properties are variable at all scales. Regional hazard maps developed for predicting site effects are generally derived from maps of surficial geology; however, recent studies have shown that mapped geologic units do not correlate well with the average shear-wave velocity of the upper 30 m, $V_s(30)$. We model the horizontal variability of near-surface soil shear-wave velocity in the San Francisco Bay Area to estimate values in unsampled locations in order to account for site effects in a continuous manner. Previous geostatistical studies of soil properties have shown horizontal correlations at the scale of meters to tens of meters while the vertical correlations are on the order of centimeters. In this paper we analyze shear-wave velocity data over regional distances and find that surface shear-wave velocity is correlated at horizontal distances up to 4 km based on data from seismic cone penetration tests and the spectral analysis of surface waves. We propose a method to map site effects by using geostatistical methods based on the shear-wave velocity correlation structure within a sedimentary basin. If used in conjunction with densely spaced shear-wave velocity profiles in regions of high seismic risk, geostatistical methods can produce reliable continuous maps of site effects.

Keywords: Site response; Geohazards; Geostatistics; Hazard mapping; SCPT; SASW; Shear-wave velocity

1. Introduction

Observations from large earthquakes (e.g. 1985 Mexico City and 1989 Loma Prieta) have shown that the stiffness of the soil at a site has a strong effect on the level of shaking. Variability in these local stiffnesses contributes to the variability of ground motions over short distances within sedimentary basins [1–5]. The engineering code has simplified these site effects into a single parameter: the average shear-wave velocity in the upper 30 m at a site, $V_s(30)$ [5]. Initial maps of site effects assign a site class, A through F, based on $V_s(30)$ measurements in each geologic unit as defined by the National Earthquake Hazards Reduction Program (NEHRP) [6].

This study seeks an appropriate model for the horizontal variability of near surface shear-wave velocity to make reliable estimates in unsampled locations. Shear-wave velocity is an important parameter because $V_s(30)$ is used to determine response spectra for building codes and detailed shear-wave velocity models are necessary for accurate ground motion modeling. Stochastic spatial models have been shown to appropriately describe the variability of soils. Fenton [7] summarizes the different stochastic models of soil properties including the sample covariance, spectral density, variance function, variogram, and wavelet variance functions. Fenton [8] used 143 cone penetration test (CPT) soundings from soil distributed over an area of 18 km^2 in which he assumes that the volume of soil is a homogeneous random field and that each sounding of tip resistance is a sample of that random field. From this study he concluded that the vertical variation of tip resistance is fractal. This implies the variability increases indefinitely as the scale of measurement increases. If the variance becomes constant at some scale, then it would be a finite variance model, and the distance at which the

*Corresponding author. Tel.: +1 617 627 3098; fax: +1 617 627 3994.
E-mail address: eric.thompson@tufts.edu (E.M. Thompson).

0267-7261/$ - see front matter © 2006 Elsevier Ltd. All rights reserved.
doi:10.1016/j.soildyn.2006.05.004

variance reaches the maximum value is called the range. The maximum variance and the range characterize the heterogeneity of a variable. Many previous studies have used similar techniques to analyze the spatial variability of soil properties and we discuss a few examples here. Elkateb et al. [9] modeled liquefaction damage with CPT measurements and assumed that the horizontal correlation structure is the same as the vertical but with an increased range. The horizontal range should be larger than vertical due to the horizontal layering of sediments. Soulie et al. [10] modeled the variability of undrained shear strength in clays and found a vertical range of 3 m and horizontal range of 30 m. DeGroot [11] compiled soil properties (including N values, tip resistance, undrained shear strength, and hydraulic conductivity) and found values for the range in the vertical direction to be between 0.5 and 3 m and the horizontal range between 15 and 30 m. These previous studies have all modeled relatively homogeneous soil deposits at the site-specific scale. The spatial extent we are interested in for regional mapping of seismic hazard is greater than an order of magnitude larger than these previous studies.

Initially, the maps of ground-motion amplification were based on previously mapped geologic units [12]. For each geologic unit, an average shear-wave velocity was determined from velocity profiles. The United States Geologic Survey (USGS) collected 210 SCPT profiles in a 140 km^2 area of the San Francisco Bay, California, which provided more detailed velocity data within each geologic unit [13]. Holzer et al. [14] produced NEHRP site class maps from these data by calculating $V_s(30)$ on a 50 m grid. The researchers set the shear-wave velocity of each geologic unit equal to the mean of the distribution of V_s values measured within each geologic unit. The shear-wave velocity profile was constructed at each node of the 50 m grid by manually contouring the thickness of each unit. They calculated $V_s(30)$ from the shear-wave velocity profile at each node. This method produced more variability of the mapped $V_s(30)$ values than regional maps based exclusively on surficial geology such as Wills et al. [6]. The variability of $V_s(30)$ in these maps results from the unit thickness contouring since the shear-wave velocity of each geologic unit is constant. Most of the profiles in this dataset do not reach depths of 30 m so this method requires extrapolation of the V_s data to depths not measured in the dataset.

As an alternative approach, we investigate the spatial variability of shear-wave velocity across geologic units within a sedimentary basin. Scott et al. [15] found that mapped geologic units do not correlate well with $V_s(30)$ measurements. The assumption of horizontal spatial homogeneity, as in the stochastic methods of Fenton [7,8] and Elkateb et al. [9] does not apply because our measurements are taken from different geologic formations such as dune sands, alluvial fans, bay mud, and artificial fill. We also do not assume that the shear-wave velocity of each geologic unit is constant.

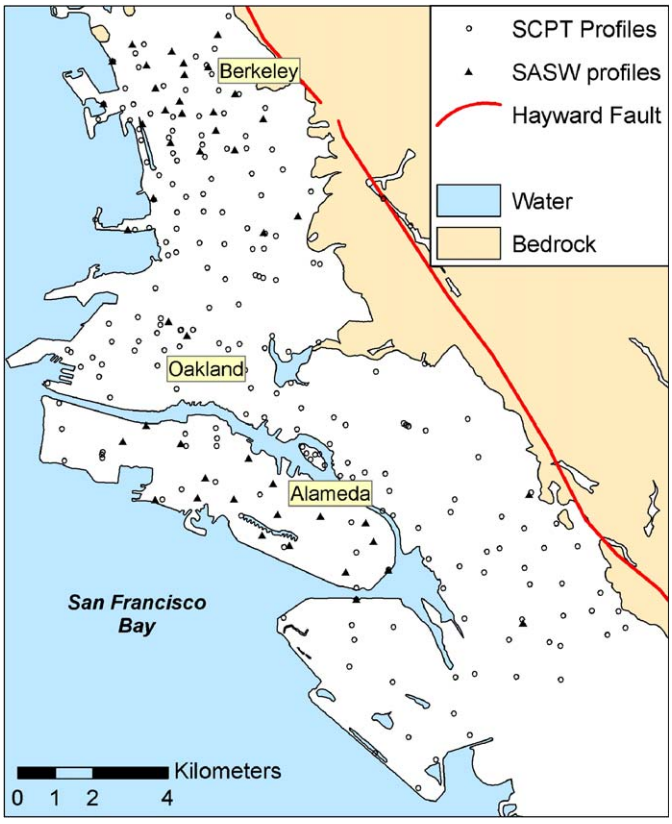

Fig. 1. Map showing the location of SCPT and SASW sites within the sedimentary basin. The SCPT data is more continuous and densely spaced than the SASW data. The SASW data is mostly grouped in two locations: near Berkeley, and near Alameda.

The two techniques used to measure shear-wave velocity in this study, seismic cone penetration test (SCPT) and spectral analysis of surface waves (SASW), each have a different role in this study. In order to map surface shear-wave velocity across a region, we need data that are densely spaced and accurately represent site response effects. The benefit of the SCPT data is that the sampling density is great enough that it can be continuously mapped. However, the measurements do not reach depths great enough to reliably characterize the $V_s(30)$. For this study, we collected 48 SASW measurements. The SASW technique accurately measures the shear-wave velocity to depths of 30 m or greater, but the 48 sites collected for this study are not as closely spaced or as spatially extensive as the SCPT data. Fig. 1 shows the measurement locations for the SASW and SCPT data used in this study. If the SASW data are strongly correlated to the SCPT data then we can use both measurements together to map seismic hazard.

2. Methods

2.1. SCPT data

The SCPT data used in this paper were collected and presented in a digital database by Holzer et al. [13]. The locations of these measurements are included in the map in

Fig. 1. As the cone is driven through the soil, the tip resistance and sleeve friction are measured at 50 mm increments and a seismometer in the tip measures seismic waves produced by a strike plate at the ground surface at depth increments of approximately 2 m. The shear-wave travel time is picked from the resulting seismogram. From the travel time data, shear-wave velocity may be calculated for the interval between each measurement. Because of uncertainty in picking shear-wave arrivals, the individual travel times may result in large errors in the calculated velocity. This is apparent because some 2-m intervals in this SCPT data have negative shear-wave velocities when calculated with this method.

As a more stable and reliable measure of shear-wave velocity, we interpret a layered velocity model for each site using automated algorithms written in the open-source statistical language and environment *R* [16]. The method is based on that described by Boore [17], but does not account for refractions at layer boundaries and assumes no prior knowledge of layer boundary depths. The ray path is approximated by a straight line which is reasonable for small horizontal surface offsets (0.96 m for these data). First, a single-layer model with thickness equal to the depth of the deepest measurement is fit to all travel times. A boundary is placed at the maximum residual in the model and travel time curves are then recalculated using the new layers. The algorithm then picks the layer with the largest root mean square (RMS) error to add a new boundary. Within this layer, the maximum residual is chosen for a new boundary. Each layer is required to include multiple travel time measurements. This is iterated until no new boundaries can be found, or the addition of another layer does not significantly reduce the RMS error of the model. Once the layer boundaries are chosen, the shear-wave velocity profile is calculated in a single inversion. We then review the residuals and add or remove boundaries manually if necessary.

From the calculated shear-wave velocity profile we need a single value of shear-wave velocity for each site for regional mapping. To be consistent with current engineering practice, we would like to use $V_s(30)$ but only about 9 of the 210 SCPT profiles reach depths of 30 m or greater. Extrapolating profiles with maximum depths less than 30 m depth can lead to incorrect site classifications and poor velocity estimates at individual sites [18]. Instead we calculate a similar value, $V_s(10)$, which is the time-weighted average shear-wave velocity, $V(d)$, of the upper d meters, with n layers with thickness Δz calculated according to the equation

$$V(d) = \frac{d}{\mathrm{tt}(d)}$$

and the travel time $\mathrm{tt}(d)$ is

$$\mathrm{tt}(d) = \sum_{i=1}^{n} \frac{\Delta z_i}{V_s(d)_i}.$$

Of the 210 original SCPT sites, we use only the190 sites in which the travel time measurements reach a minimum depth of 10 m. Of these 190 sites, we remove one from our analysis because it is collocated with another site.

2.2. SASW data

For this study we collected 48 SASW measurements in the same area as the SCPT data. The locations of the SASW measurements are included on the map in Fig. 1. We use the SASW method to measure soil stiffness because it can be efficiently performed in urban areas. A recent blind comparison of seismic methods showed that the SASW method applied in this study produces accurate shear-wave velocity profiles and can identify low-velocity layers in the near-surface sediments [19]. We chose locations at public parks where possible, but otherwise the accelerometer arrays are placed on the sidewalks of city streets.

We generate surface waves by vertically loading the soil with an electro-mechanical shaker driven at discrete harmonic frequencies between 2 and 200 Hz. We arrange the 4 accelerometers according to the common source-midpoint geometry illustrated in Fig. 2. These accelerometers measure the vertical acceleration time series produced by the harmonic vertical loading. We calculate the phase angle (ϕ, in radians) from the cross power spectra of two accelerometers. From the phase, and the separation distance between the seismometers, d, we can calculate the wavelength, $\lambda = 2\pi d/\phi$. At each site we collect phase data with accelerometer spacing from 2 to 50 m. The source to receiver distance is always greater than or equal to the distance between accelerometers to minimize the near-field effects [20]. From the frequency and the wavelength we calculate the Rayleigh wave velocity,

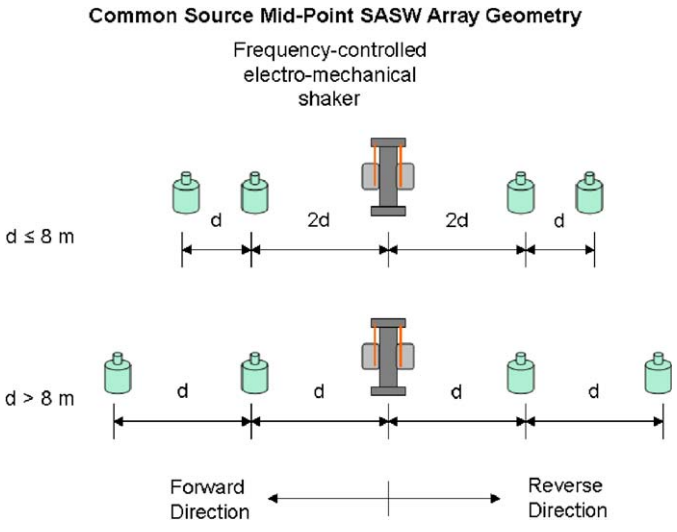

Fig. 2. The schematic layout of the common source mid-point SASW array used in this study. The forward and reverse accelerometer pair for each spacing records the surface waves produced by the harmonic source located at the center.

$V_r = f\lambda$. At each site, we combine the velocity and wavelength data from each array spacing to calculate an average dispersion curve (the relationship of surface wave velocity vs. wavelength) for each site.

We find layered velocity model that produces the best-fit theoretical dispersion curve by minimizing the sum of the squares of the residuals relative to the experimental dispersion curve measured in the field. We use the algorithm WaveEQ by OYO Corp [21] to invert for the layered velocity model from the experimental dispersion curve. This is an automated-numerical approach that uses a constrained least-squares fit of the theoretical and experimental dispersion curves. With this dataset, we invert for the shear-wave velocity profile in the upper 30 m of the soil unless the maximum wavelength of the experimental dispersion curve is greater than 90 m, in which case we increase the depth of the inversion profile to the maximum wavelength of the experimental dispersion curve divided by three ($\lambda_{max}/3$). Most profiles contain 6–8 layers unless the addition of more layers is required to fit the shape of the experimental dispersion curve. Multiple inversions are fit to the experimental dispersion curves by adjusting the parameters (such as the initial velocity model, the number of layers, etc.) to verify that the solution is stable.

2.3. Geostatistics

We presume that the SCPT and SASW measurements are densely spaced enough that the V_s values are not random in the sense that closely spaced observations will be more similar than those further apart. Geostatistics is an appropriate tool for spatial prediction and stochastic simulation of data if this spatial structure exists. The experimental semivariogram (described below) describes the spatial structure, and using a suitable semivariogram model to interpolate between data points can significantly reduce the variance of predicted values. We use the geoR package [22] within the statistical language and environment *R* for the geostatistical calculations. The empirical semivariogram, $\gamma(h)$, with N sample pairs separated at a distance of h is estimated by the following equation:

$$\gamma(h) = \frac{1}{2N}\sum_{i=1}^{N}[V_s(s_{i+h}) - V_s(s_i)]^2,$$

where s is the spatial location of the velocity measurement, V_s. The sample pairs are divided into bins of separation distance. We fit a model semivariogram to the empirical semivariogram and find that exponential and linear models are appropriate for the data in this study. The exponential model has the form:

$$\tilde{\gamma}(h) = \omega\left[1 - \exp\left(-\frac{h}{a}\right)\right] + \tau$$

and the linear model has the form

$$\tilde{\gamma}(h) = m[h] + \tau.$$

The model parameters are found by minimizing the weighted least-square error as described by Cressie [23]. The nugget variance is τ, the range is $3a$, and the sill variance ($\tilde{\sigma}^2$), is $\omega + C$. Graphically, the sill variance is the value at which the semivariogram plateaus as the distance increases and it is equivalent to the population variance of the variable. The range is the distance at which the semivariogram reaches the sill, and points at distances larger than the range are not correlated. The nugget variance is the variance at the origin, or separation distance of 0. The nugget variance characterizes the continuity of the variable being modeled. A flat empirical semivariogram is characteristic of a purely random variable with no correlation structure. Geostatistics cannot improve estimates of a purely random variable. The linear model does not contain the parameters a or ω because the range and sill are infinite. The slope of the linear model is m, and the nugget variance is τ.

We include the equations necessary for describing the soil variability above and recommend the reader to any of the well-written texts on the subject (e.g. [24,25]) for further details of the geostatistical modeling.

3. Results

3.1. Comparison of SCPT and SASW methods

The two measurements of shear-wave velocity used in this paper are inherently different. Fig. 3 presents closely

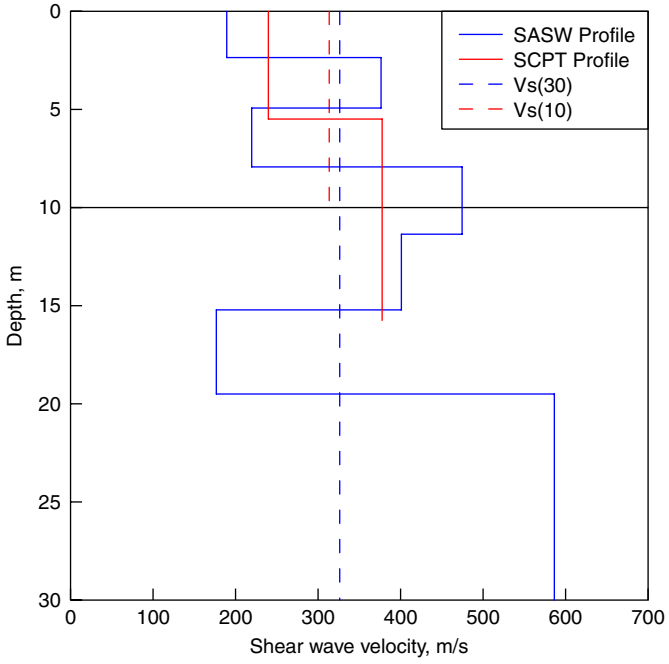

Fig. 3. Two shear-wave velocity profiles measured by the SASW and SCPT methods located within 100 m of each other. The SASW method effectively averages the shear-wave velocity over the volume of sediment through which the surface wave travel (up to 200 m for these data), while the SCPT method measures the shear-wave velocity along a single vertical raypath.

spaced shear-wave velocity profiles measured by the SCPT and SASW methods and the corresponding $V_s(10)$ and $V_s(30)$ values. These two sites are separated by approximately 100 m. There is no reason to expect that these profiles should be identical, so the purpose of this figure is to compare the nature of the two methods and not the absolute values of the profiles. The SCPT method more directly measures shear-wave velocity in the sense that it divides the time for the shear-wave to arrive by the distance traveled. On the other hand, the SASW method is measuring the dispersion of surface waves and the shear-wave velocity is calculated by inverse methods which yield a non-unique solution. Further, the SASW method is effectively averaging the soil properties over the volume of sediment through which the surface wave travel (up to 200 m for these data), while the SCPT method effectively measures the shear-wave velocity for a single vertical raypath. From the two profiles, it is apparent that the SASW technique produces greater detail, but this is controlled by the inversion process in which the number of layers is specified. The SCPT method measures shear-wave arrivals every 2 m, and so it cannot resolve changes in the shear-wave velocity profile at scales equivalent to 4 m or less. For example, the upper layer in the SCPT profile in Fig. 3 is defined by only two measurements, and the lower layer is defined by 6. These velocities may actually represent the average shear-wave velocity of thinner layers which cannot be resolved. The SASW dispersion curve is compiled from multiple receiver spacings (typically 2 arrays, each with 5–6 different spacings from 2 to 50 m), each spacing measures the phase at 30–60 wavelengths (wavelength determines the depth of particle motion in the Rayleigh wave). Thus, the SASW method measures the shear-wave velocity more continuously with depth and the precision of the SASW profile should be greater than the SCPT profile. A blind comparison of shear-wave velocity measurement techniques [19] found that the SCPT method is biased by 15% high relative to suspension log data and that the SASW method used in this study is unbiased in the upper 20 m and showed a bias to high velocities at greater depths.

3.2. Semivariogram estimation

Fig. 4 shows the experimental and model semivariograms for the SASW and SCPT data. We use 400 m distance bins for the 190 SCPT measurements and calculate the exponential model parameters: the nugget variance is 80 m^2/s^2, the sill variance is 5204 m^2/s^2, and the range is approximately 3.7 km. This model fits the empirical data well and the nugget variance is small relative to the sill variance demonstrating that high correlations exist over short horizontal distances. We use a larger bin size of 1 km for the SASW data because it is less closely spaced and there are fewer measurements. The SASW data are best fit with a linear covariance model with nugget variance.

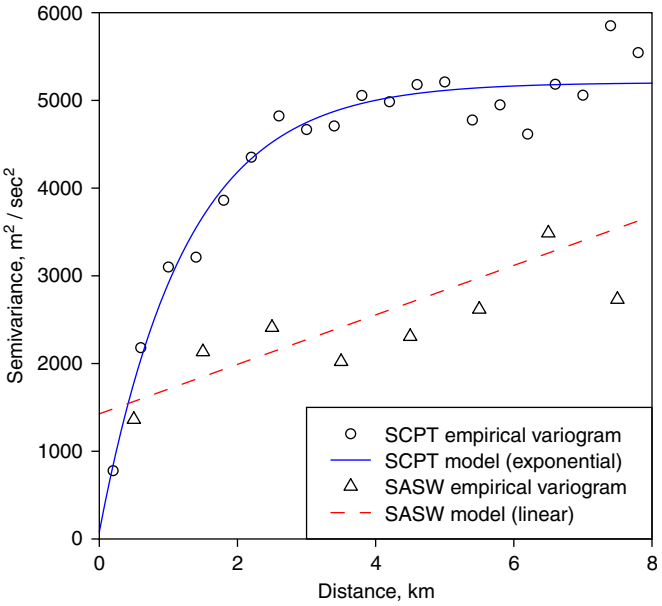

Fig. 4. The experimental and model semivariograms for the SCPT and the SASW data. The model SCPT variogram is exponential, and the model SASW semivariogram is linear. The semivariance of the SASW data is smaller than the semivariance of the SCPT data at all distances, but the SASW data does not have enough closely spaced measurements to constrain the shape of the semivariogram at small separation distances.

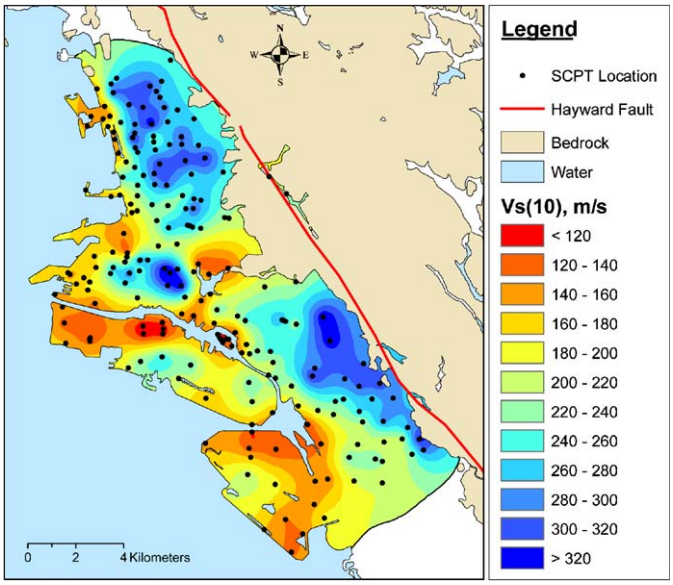

Fig. 5. Continuous map of $V_s(10)$ based on the SCPT data collected by Holzer et al. [13].

The nugget variance is 1427 m^2/s^2 and the line has a slope of 0.28.

We estimate $V_s(10)$ values everywhere within the region contained by the SCPT measurements in a 100 m grid with ordinary kriging and the model semivariogram for the $V_s(10)$ values. These results are shown in Fig. 5. We only calculate estimated values within the sedimentary basin where the variance of the prediction is less than the population variance of the $V_s(10)$ values.

3.3. Sampling density

To address the effect of sampling density on the estimated spatial correlation structure we use a Monte Carlo simulation to produce random subsets of the data from which we calculate the model semivariogram. This is relevant to geohazards mapping because it directly addresses the horizontal sample density that should be required to map site-response. From the original 189 SCPT samples, each realization uses a random subset such that every sample has equal probability of selection and can only be used once per realization. For each sample density we calculate the nugget variance, range, and sill variance for the exponential semivariogram for 100 realizations. Fig. 6 plots the mean of (A) the nugget variance, (B) the range, and (C) sill variance for 5000 realizations at each sampling density. The selection of each semivariogram model was automated because of the large number of realizations required for a meaningful Monte Carlo simulation.

Fig. 7 shows 100 example realization of the experimental variogram with 1.2 samples per km^2 (170 samples) and 0.79 (110 samples) samples per km^2. This figure shows that as the sampling density decreases, the standard deviation of the nugget variance, the range, and the sill variance increase. Interestingly, all three of the variogram model parameters increase at a relatively constant rate as the sampling density decreases. This results from the model variogram being less well constrained by the empirical variogram. Fig. 6 shows that the values of the range and sill variance increases distinctly as the sampling density is decreased below 0.85 samples/km^2. The reason for this change is that at the lower sampling densities, some of the realizations of the experimental semivariogram appear linear. Since the linear experimental semivariogram is fit automatically with an exponential model, the values for the model range and sill become unrealistically large. Therefore, the large jump in Fig. 7 represents a breakdown in the assumption of an exponential model. To illustrate this, Fig. 8 shows the histograms of the nugget variance, range,

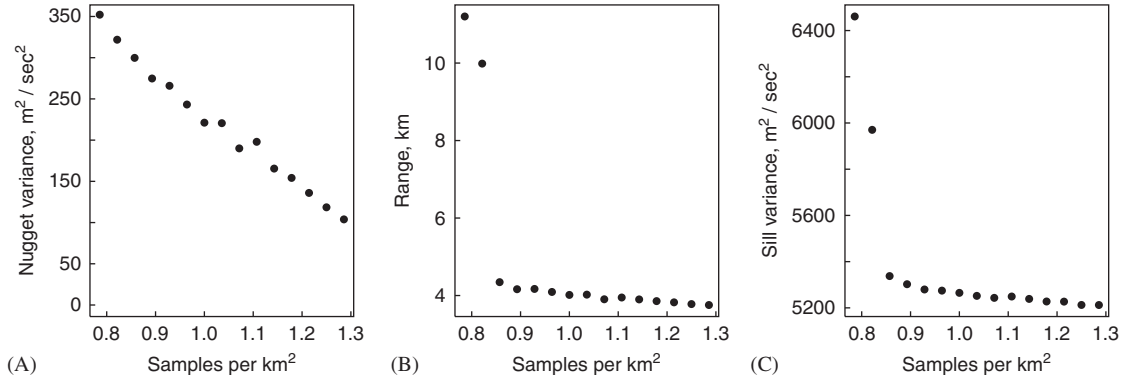

Fig. 6. $V_s(10)$ semivariogram parameters from Monte Carlo simulations in which the sampling density is varied. These plots show how (A) nugget variance, (B) range, and (C) sill variance change as a function of sampling density. The nugget variance increases approximately linearly as sampling density is decreased. The range and sill variance both increase slightly as the sampling density decreases until a critical value at approximately 0.85 samples/km^2 where there is a distinct increase in value of both.

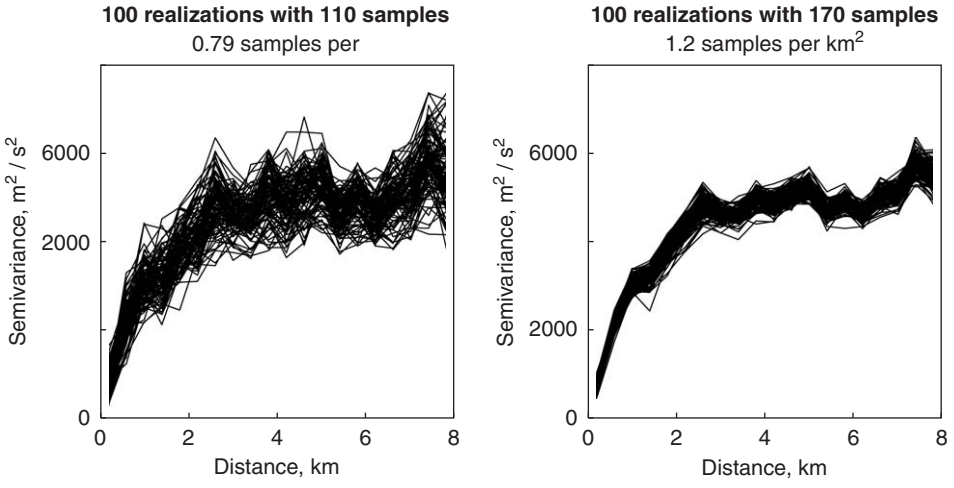

Fig. 7. Empirical semivariograms for 100 realizations of the Monte Carlo simulation with (A) 110 samples, which has a sampling density of 0.79 samples/km^2, and (B) 170 samples, which has a sampling density of 1.2 samples/km^2.

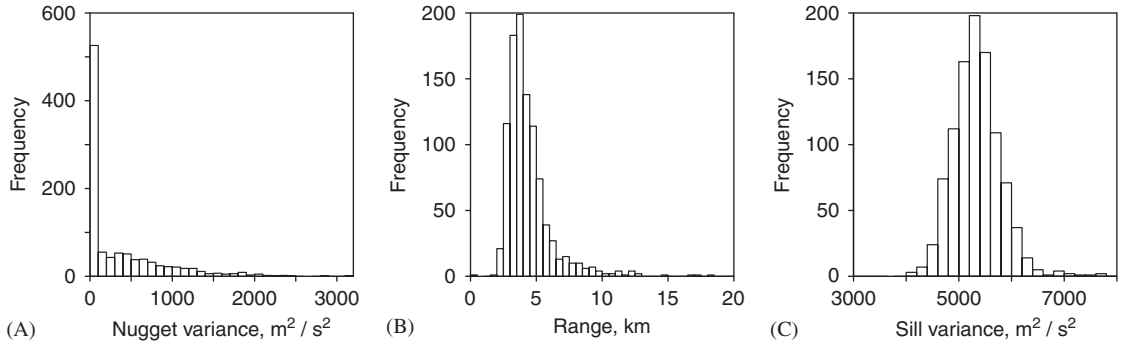

Fig. 8. Histograms of (A) nugget variance, (B) range, and (C) sill variance calculated from the 0.79 samples/km^2 Monte Carlo simulation.

and sill variance calculated from the 0.79 samples/km^2 Monte Carlo simulation (110 samples). The median of the range is 3.96 km, and the maximum value is greater than 2000 km, which is an unrealistic value for the simple reason that it is greater than the spatial extent of the dataset. The median of the sill variance is 5314 m^2/s^2 but the maximum sill variance is approximately 356,000 m^2/s^2 which is similarly unrealistic because it is greater than the population variance of the data. These outliers are not valid models and indicate that while most of the realizations with 0.79 samples/km^2 are reasonable, some appear linear and should not be fit with an exponential semivariogram model.

4. Discussion

Although geologic units are often used for mapping sediment shear-wave velocities, geologic units may not be appropriate shear-wave velocity boundaries because different geologic units can contain sediments with similar shear-wave velocities. Fig. 9 shows the probability density functions of shear-wave velocity for each geologic unit from the SCPT study of Holzer et al. [26]. This figure shows that the distributions are broad and there is significant overlap between different geologic units. Most shear-wave velocity measurements could likely be located within more than one geologic unit and the geologic unit does not accurately determine the shear-wave velocity.

The range in the horizontal correlation structure of the sediments studied in this paper is approximately two orders of magnitude larger than most previous studies that use geostatistical methods to model soil properties. The physical properties measured in the previous studies are effectively point data (such as tip resistance or undrained shear strength) whereas we use the shear-wave velocity averaged over a large volume of sediment. The spatial coverage and separation distance of the data in this study is not capable of resolving correlations at the smaller scales of these previous studies. For the $V_s(10)$ data, we find that the variance continues to increase at separation distances up to approximately 4 km. We do not find that the variance of $V_s(30)$ flattens at any distance measured. This suggests that it may be fractal. However, the spacing between SASW

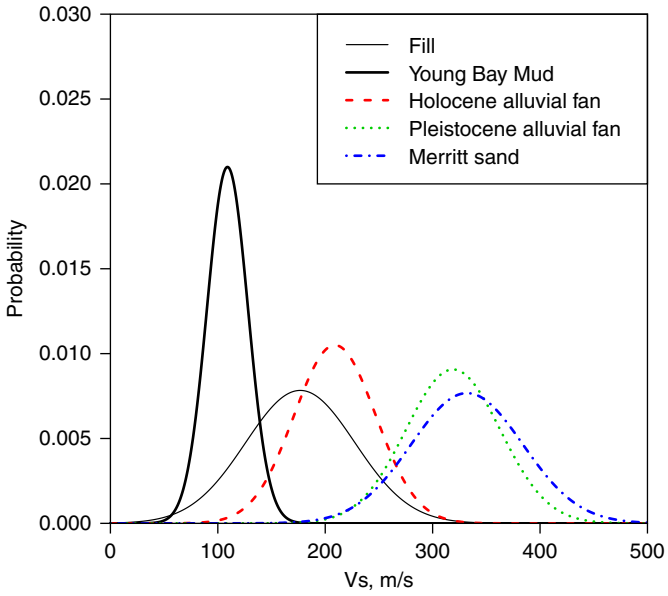

Fig. 9. Probability density functions of shear wave velocity for different geologics. Data originally presented by Holzer et al. [25]. The distributions are broad relative to the difference between the means.

measurements does not provide sufficient data to constrain the model below 1 km or beyond about 5 km. The Monte Carlo simulation described above shows that this type of semivariogram could be produced from an exponential distribution of velocity that was not sampled densely enough. Therefore, a more densely spaced dataset would provide more conclusive results.

The variance of $V_s(30)$ is lower than $V_s(10)$ at all separation distances. This could be because $V_s(30)$ is inherently less variable than $V_s(10)$ as a result of the larger "size" of the $V_s(30)$ measurement. Alternatively, the $V_s(30)$ semivariogram may be less well constrained because there are fewer measurements and the spatial coverage is less continuous. If the latter were true and we had a more extensive dataset of SASW measurements then the linear shape of the $V_s(30)$ semivariogram may become more similar to the exponential shape of the $V_s(10)$ semivariogram.

Fig. 5 illustrates how geostatistical methods can be used to produce a more detailed and accurate map of

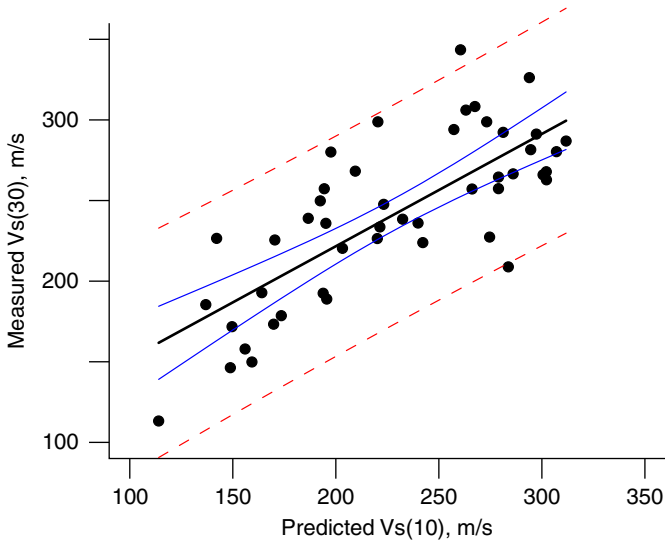

Fig. 10. Comparison of $V_s(10)$ and $V_s(30)$ measurements. The $V_s(10)$ values are estimated by kriging at the location of each $V_s(30)$ measurement and plotted against the measured $V_s(30)$ values. The solid lines are the linear model and confidence interval, and the dashed lines are the 95% tolerance interval.

shear-wave velocity. Current site effects maps are limited to the range of $V_s(30)$ values that define each NEHRP site class (180 m/s or greater for each site class) and by previously mapped boundaries based on geologic units. As more data are collected, researchers are finding that geologic boundaries are inappropriate site class boundaries [15]. Site class boundaries derived from a map of kriged $V_s(30)$ measurements should be more reliable because it is based on the empirical velocity structure of the sediments rather than mapped geologic units.

Although we have enough measurements of $V_s(10)$ to map continuously, it is not a reliable measurement of site response. It would therefore be useful if we could relate the $V_s(10)$ values to $V_s(30)$. At each $V_s(30)$ measurement location, we estimate the $V_s(10)$ using ordinary kriging. Fig. 10 plots $V_s(10)$ against $V_s(30)$. The figure includes the linear model with the associated 95% confidence interval (solid lines) and the 95% tolerance interval (dashed lines). The intervals show that $V_s(10)$ is weakly correlated to $V_s(30)$ and that $V_s(10)$ can only predict $V_s(30)$ to within about 70 m/s. Unfortunately, the magnitude of the error in predicting $V_s(30)$ from $V_s(10)$ is too large to produce meaningful maps of site response.

5. Conclusions

The SCPT $V_s(10)$ measurements and SASW $V_s(30)$ measurements each have a different function in this paper. Previous studies have correlated $V_s(30)$ with ground motion amplification factors. However, measurements of $V_s(30)$ are typically expensive and time consuming to collect. The $V_s(30)$ measurements discussed herein are sparse and we are not able to determine an appropriate semivariogram model especially at small and large separation distances. The $V_s(10)$ data are important because the sample locations are densely spaced, resulting in a clear characterization of the shear-wave velocity correlation structure. Because $V_s(30)$ is the same physical property as $V_s(10)$ but extended to greater depths, we expect that $V_s(30)$ should exhibit a similar correlation structure as $V_s(10)$. Fig. 4 shows that the correlation of $V_s(30)$ is greater than that of $V_s(10)$ at all separation distances and appears to be linear while the $V_s(10)$ correlation structure is exponential. This could be due to the difference in sampling density, because the characteristic size of the measurements are different, or simply because the correlation structure of the sediments at greater depths is different.

Continuous mapping of $V_s(30)$ would help identify localized areas of high seismic risk in urbanized areas. The soil properties can change the amplitude and frequency content of ground motions over short horizontal distances which can cause severe damage to structures adjacent to undamaged areas. This study demonstrates that shear-wave velocity of the upper 10 m of soil exhibit horizontal correlations at distances of up to 4 km. Since shallower measurements of shear-wave velocity cannot accurately predict $V_s(30)$, $V_s(30)$ must be measured directly.

Acknowledgments

This research was partially funded by National Science Foundation Grant CMS-0409311 and a Dean's Summer Scholarship from Tufts University. The Coastal and Marine Geology program of the United States Geological Survey provided the field equipment and funded the collection the SASW data presented in this paper. The authors would like to thank Dave Boore for his advice on the interpretation SCPT travel time data.

References

[1] Borcherdt RD. Effects of local geology on ground motion near San-Francisco-Bay. Bull Seismol Soc Am 1970;60(1):29.
[2] Borcherdt RD, Gibbs JF. Effects of local geological conditions in the San Francisco Bay region on ground motions and the intensities of the 1906 earthquake. Bull Seismol Soc Am 1976;66(2):467.
[3] Hanks TC, Brady AG. The Loma-Prieta earthquake, ground motion, and damage in Oakland, Treasure-Island, and San-Francisco. Bull Seismol Soc Am 1991;81(5):2019.
[4] Rodriguez-Marek A, Bray JD, Abrahamson NA. An empirical geotechnical seismic site response procedure. Earthquake Spectra 2001;17(1):65.
[5] Dobry R, Borcherdt RD, Crouse CB, Idriss IM, Joyner WB, Martin GR, Power MS, Rinne EE, Seed RB. New site coefficients and site classification system used in recent building seismic code provisions. Earthquake Spectra 2000;16(1):41.
[6] Wills CJ, Petersen M, Bryant WA, Reichle M, Saucedo GJ, Tan S, Taylor G, Treiman J. A site-conditions map for California based on geology and shear-wave velocity. Bull Seismol Soc Am 2000;90 (6 PT B):187.
[7] Fenton GA. Random field modeling of CPT data. J Geotech Geoenviron Eng 1999;125(6):486.

[8] Fenton GA. Estimation for stochastic soil models. J Geotech Geoenviron Eng 1999;125(6):470.
[9] Elkateb T, Chalaturnyk R, Robertson PK. Simplified geostatistical analysis of earthquake-induced ground response at the wildlife site, California, USA. Can Geotech J 2003;40(1):16.
[10] Soulie M, Montes P, Silvestri V. Modeling spatial variability of soil parameters. Can Geotech J 1990;27(5):617.
[11] DeGroot DJ. Analyzing spatial variability of in situ soil properties. Proceedings of the 1996 conference on uncertainty in the geologic environment, Uncertainty'96. Part 1 (of 2), 31 July–3 August 1996. New York, USA: ASCE.
[12] Wills CJ, Silva W. Shear-wave velocity characteristics of geologic units in California. Earthquake Spectra 1998;14(3):533.
[13] Holzer TL, Bennett MJ, Noce TE, Padovani AC, Tinsley III JC. Liquefaction hazard and shaking amplification maps of alameda, Berkeley, Emeryville, Oakland, and Piedmont, California: a digital database, US Geological Survey Open File Report 2002; 02-296.
[14] Holzer TL, Padovani AC, Bennett MJ, Noce TE, Tinsley III JC. Mapping NEHRP $V_s(30)$ site classes. Earthquake Spectra 2005;21(2): 353.
[15] Scott JB, Clark M, Rennie T, Pancha A, Park H, Louie JN. A shallow shear-wave velocity transect across the Reno, Nevada, area basin. Bull Seismol Soc Am 2004;94(6):2222.
[16] R Development Core Team. R: a language and environment for statistical computing. R Foundation for Statistical Computing.
[17] Boore DM. A compendium of P- and S-wave velocities from surface-to-borehole logging: summary and reanalysis of previously published data and analysis of unpugblished data, US Geological Survey Open File Report 2003; 03-191.
[18] Boore DM. Estimating $V_s(30)$ (or NEHRP site classes) from shallow velocity models (depths less than or equal 30 m). Bull Seismol Soc Am 2004;94(2):591.
[19] Asten MW, Boore DM. Asten MW, Boore DM. Comparison of shear-velocity profiles of unconsolidated sediments near the Coyote Borehole (CCOC) measured with fourteen invasive and non-invasive methods. US Geological Survey Open-File Report 2005-11691.
[20] Sanchez-Salinero I, Roesset JM, Shao K, Stokoe KH, Rix GJ. Analytical evaluation of variables affecting surface wave testing of pavements. Transp Res Rec 1987(1136):86.
[21] Hayashi K, Kayen RE. Comparative test of three surface wave methods at Williams Street Park in San Jose, USA, University of Tokyo, Japan. In: 2003 joint meeting of Japan earth and planetary science, 26–29 May 2003.
[22] Ribeiro Jr. PJ, Diggle PJ. geoR: a package for geostatistical analysis. R-News 2001;1(2):15–8.
[23] Cressie NAC. Fitting variogram models by weighted least squares. Math Geol 1985;17(5):563.
[24] Isaaks EH, Srivastava RM. Applied geostatistics. New York: Oxford University Press; 1989.
[25] Cressie NAC. Statistics for spatial data. New York: Wiley; 1993.
[26] Holzer TL, Bennett MJ, Noce TE, Tinsley III JC. Shear-wave velocity of surficial geologic sediments in Northern California: statistical distributions and depth dependence. Earthquake Spectra 2005;21(1):161.